The yeast C/D box snoRNA U14 adopts a "weak" K-turn like conformation recognized by the Snu13 core protein in solution

Marie-Eve Chagot, Marc Quinternet, Benjamin Rothé, Bruno Charpentier, Jérôme Coutant, Xavier Manival, Isabelle Lebars

Biochimie 164 (2019) 70–82

Contents lists available at ScienceDirect

Biochimie

journal homepage: www.elsevier.com/locate/biochi

Research paper

The yeast C/D box snoRNA U14 adopts a "weak" K-turn like conformation recognized by the Snu13 core protein in solution

Marie-Eve Chagot [a], Marc Quinternet [b], Benjamin Rothé [a, 1], Bruno Charpentier [a], Jérôme Coutant [c], Xavier Manival [a, **], Isabelle Lebars [d, *]

[a] CNRS, IMoPA, Université de Lorraine, Nancy, F-54000, France
[b] CNRS, INSERM, IBSLOR, Université de Lorraine, Nancy, F-54000, France
[c] Bruker France, 34 rue de l'Industrie, BP 10002, 67166, Wissembourg Cedex, France
[d] Structure and Dynamics of Biomolecular Machines, Université de Strasbourg, CNRS, Architecture & Réactivité de l'ARN, UPR 9002, Institut de Biologie Moléculaire et Cellulaire (IBMC), 15 rue René Descartes, F-67000, Strasbourg, France

ARTICLE INFO

Article history:
Received 6 December 2018
Accepted 20 March 2019
Available online 23 March 2019

Keywords:
snoRNA U14
K-turn
Snu13 protein
NMR

ABSTRACT

Non-coding RNAs associate with proteins to form ribonucleoproteins (RNPs), such as ribosome, box C/D snoRNPs, H/ACA snoRNPs, ribonuclease P, telomerase and spliceosome to ensure cell viability. The assembly of these RNA-protein complexes relies on the ability of the RNA to adopt the correct bound conformation. K-turn motifs represent ubiquitous binding platform for proteins found in several cellular environment. This structural motif has an internal three-nucleotide bulge flanked on its 3′ side by a G•A/A•G tandem pairs followed by one or two non-Watson-Crick pairs, and on its 5′ side by a classical RNA helix. This peculiar arrangement induces a strong curvature of the phosphodiester backbone, which makes it conducive to multiple tertiary interactions. SNU13/Snu13p (Human/Yeast) binds specifically the U14 C/D box snoRNA K-turn sequence motif. This event is the prerequisite to promote the assembly of the RNP, which contains NOP58/Nop58 and NOP56/Nop56 core proteins and the 2′-*O*-methyl-transferase, Fibrillarin/Nop1p. The U14 small nucleolar RNA is a conserved non-coding RNA found in yeast and vertebrates required for the pre-rRNA maturation and ribose methylation. Here, we report the solution structure of the free U14 snoRNA K-turn motif (kt-U14) as determined by Nuclear Magnetic Resonance. We demonstrate that a major fraction of free kt-U14 adopts a pre-folded conformation similar to protein bound K-turn, even in the absence of divalent ions. In contrast to the kt-U4 or *tyrS* RNA, kt-U14 displays a sharp bent in the phosphodiester backbone. The U•U and G•A tandem base pairs are formed through weak hydrogen bonds. Finally, we show that the structure of kt-U14 is stabilized upon Snu13p binding. The structure of the free U14 RNA is the first reference example for the canonical motifs of the C/D box snoRNA family.

1. Introduction

In the cell, RNA molecules associate with proteins to form ribonucleoproteins (RNPs) such as ribosome and spliceosome to ensure cell viability. The assembly of these RNA-protein complexes relies on the ability of the RNA to adopt the correct bound conformation, an event that generally requires the intervention of co-factors. Understanding the sequence-structure-function relationships in RNPs requires three-dimensional structural information on RNA molecules, both in presence and absence of their binding partners (proteins) or cofactors (metal ions).

1.1. The kink-turn motif

The kink-turn or K-turn motifs are universal structural elements found in ribosomal RNAs (rRNAs) [1], small nuclear RNAs (snRNAs) [2], small nucleolar RNAs (snoRNAs) [3], SelenoCystein Insertion

* Corresponding author.
** Corresponding author.
E-mail addresses: xavier.manival@univ-lorraine.fr (X. Manival), i.lebars@ibmc-cnrs.unistra.fr (I. Lebars).
[1] Present address: Benjamin Rothé, Ecole Polytechnique Fédérale de Lausanne (EPFL) SV ISREC, Station 19, CH-1015 Lausanne, Switzerland.

https://doi.org/10.1016/j.biochi.2019.03.014
0300-9084/

Sequence (SECIS) of the 3′-untranslated regions of selenoprotein mRNA [4,5], and 5′ UTRs including several riboswitches [6,7]. They consist of a three-nucleotides internal loop flanked on its 3′ side by a G•A/A•G tandem pairs followed by one or two non-Watson-Crick pairs (NC), and on its 5′ side by a conventionally base-paired helix (C) (Fig. 1A). This peculiar arrangement induces a strong curvature of the phosphodiester backbone between the two helices leading to a compact structure thanks to near-universal A-minor tertiary interactions [8,9]. There are two classes of K-turn structure depending on whether the O2′-H of the ribose at the *-2* position establishes hydrogen bonds with the N3 or N1 of the A_5 cycle (Fig. 1A). The modification of the hydrogen bond network involves a different rotation of the A_5 nucleobase that affects its conserved base-pairing with G_6 and changes the whole shape of the K-turn structure. The first and second unpaired residues (N_1 and N_2, Fig. 1A) are stacked on the C and NC helices, respectively. The third unpaired residue (N_3, Fig. 1A), which is fully exposed to the solvent, represents a key interaction determinant for K-turn binding proteins.

1.2. The C/D box snoRNA family

Small nucleolar RNAs found in Archaea and Eukaryotes guide chemical modifications of ribosomal RNAs (rRNA), transfer RNAs (tRNA) and small nuclear RNAs (snRNA). The C/D box snoRNAs are associated with 2′-*O*-methylation of rRNA. They are characterized by the presence of conserved sequences, termed boxes C (5′-RUGAUGA-3′, where R is a purine) and D (5′-CUGA-3′), located near the 5′ and 3′ ends of the snoRNA, respectively (Fig. 1B). The C/D box folds into a K-turn through pairing between regions upstream of the C box and downstream of the D box, that are brought in close proximity [10]. The C/D box K-turn is a key player in methylation and processing of rRNA, stability and localization of snoRNPs. In an early stage during box C/D snoRNP assembly, the recruitment of the L7Ae protein [11,12] or SNU13/Snu13 protein (Human/Yeast) initiates the assembly process by binding specifically the K-turn motif of snoRNAs [13–15]. In particular, SNU13/Snu13p binds specifically the U14 snoRNA, a prerequisite for the successive arrival of the other constituents of the ribonucleoparticle, namely in eukaryotes, the proteins NOP58/Nop58 and NOP56/Nop56 and the 2′-*O*-methyltransferase, Fibrillarin/Nop1p [14,15].

1.3. The U14 snoRNA

As U3 snoRNA, the U14 snoRNA is a conserved non-coding RNA found in yeast and vertebrates required for the pre-rRNA maturation. Genetic depletion studies in *S. cerevisiae* showed that C/D box snoRNA U3, and U14 (also named snR128) are essential for cell viability and required for the 35S pre-rRNA cleavages that release the 18S rRNA [16,17]. Analyses of U14 sequences revealed the presence of a conserved terminal helix and five universal sequence elements: C and D boxes corresponding to a K-turn sequence motif, and A, B, and Y domains (Fig. 1B). A second set of boxes, the C′/D′,

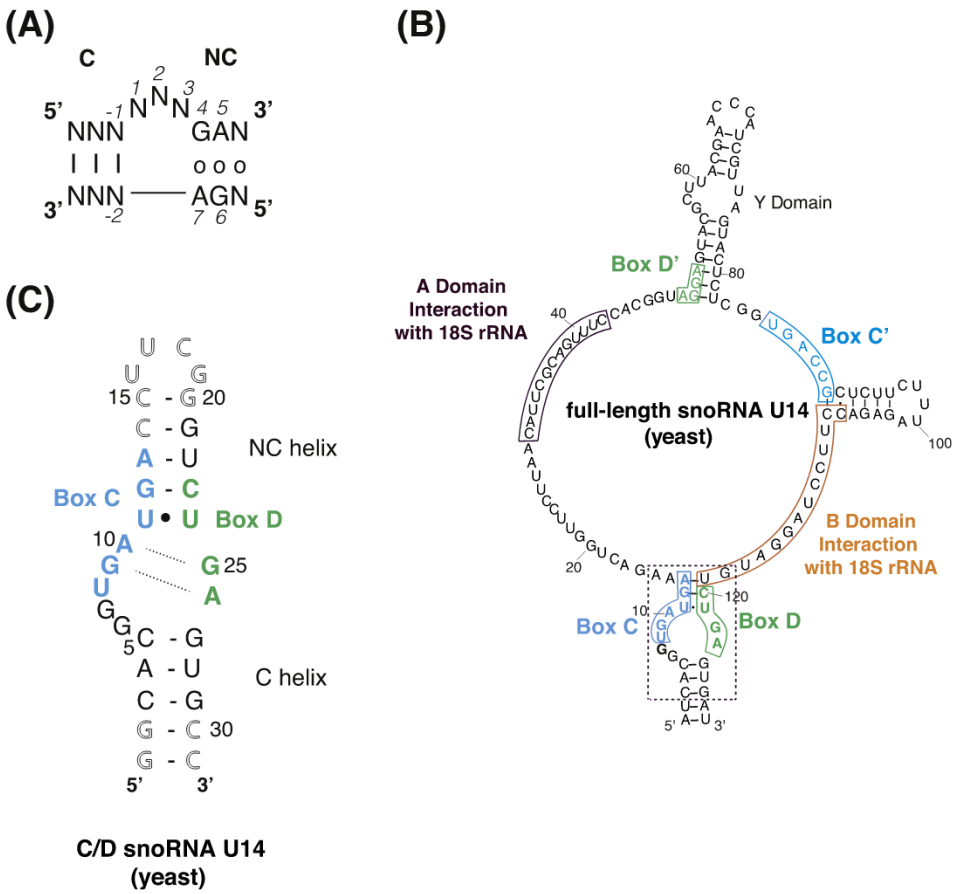

Fig. 1. The U14 snoRNA from *S. cerevisiae*. **(A)** Secondary structure of consensus k-turns. Canonical and non-canonical stems are indicated by C and NC respectively. The numbering of the internal bulge is in italic. **(B)** Secondary structure of full length U14 from *S. cerevisiae* (adapted from Ref. [79]). The sequences of the boxes C/C′ and D/D′ are shown in blue and green respectively (adapted from Ref. [18]). Domains A, B, and Y are also represented. **(C)** Secondary structure of terminal conserved boxes C and D from the U14 snoRNA used for NMR studies. The numbering of the RNA is indicated. The nucleotides represented in outline are not naturals.

has been recently identified [18]. Base pairing of A, B and Y domains of U14 with the 18S rRNA is required for the synthesis of functional ribosomes in yeast [19–21] suggesting that U14 contributes directly to rRNA processing. Moreover, the B domain of both vertebrate and yeast U14 snoRNAs is complementary to a sequence in 18S rRNA region that contains validated 2′-*O*-methylation at nucleotide C414 (UMASS Amherst Yeast snoRNA Database). In *Xenopus laevis*, depletion of the U14 snoRNA prevents 2′-*O*-methylation of 18S rRNA and an intact B domain is essential for the methylation [22]. Altogether, the snoRNP U14 would therefore have the dual function in rRNA maturation and ribose methylation.

Here, we report the solution structure of the free U14 snoRNA K-turn motif determined by Nuclear Magnetic Resonance (NMR). We demonstrate that a major fraction of U14 adopts a pre-folded conformation similar to known bound K-turn, even in the absence of protein or divalent ions. Finally, we show that the structure of kt-U14 is stabilized upon Snu13p binding. This first structural characterization of a free canonical C/D motif can serve as a reference for the C/D box snoRNA family. Its comparison with other family members allows discussing the consequences of this pre-folded k-turn during the snoRNP assembly and the relevance of an external scaffold.

2. Materials and methods

2.1. RNA samples preparation

Milligram quantities of RNAs were prepared both unlabeled and uniformly $^{13}C/^{15}N$ labeled by *in vitro* transcription with in-house T7 RNA polymerase from oligonucleotide templates [23]. The DNA templates were purchased from Eurogentec (France). Labeled NTPs (nucleotide triphosphate) were purchased from SIGMA-ALDRICH (USA). Transcription conditions were optimized with varying magnesium concentrations in 25 μL reaction mixtures in 40 mM TRIS-HCl pH 8, 1 mM spermidine, 0.01% Triton X-100, 5 mM DTT and 10% polyethylene glycol (PEG8000), in the presence of 4 mM of each NTP [23,24]. Preparative *in vitro* transcriptions were next performed with 16 mM $MgCl_2$ in 5 mL reaction volumes. The reaction mixture was incubated at 37 °C during 4.5 h. After phenol extraction and ethanol precipitation, RNAs were next purified by FPLC or on denaturing polyacrylamide gels followed by electro-elution [24]. After ethanol precipitation, RNAs were dialyzed for 24 h against the buffer used for NMR experiments. Samples were concentrated by lyophilization and resuspended in 90%/10% H_2O/D_2O for experiments involving exchangeable protons and in 99.9% D_2O for non-exchangeable proton experiments. Each sample was refolded by heating at 95 °C (2 min) and snap-cooled at 4 °C. The concentration of RNA samples was measured using a Nanodrop Spectrometer and calculated with molar extinction coefficients.

2.2. Expression and purification of Snu13p

The *E. coli* BL21(DE3) strain (Novagen) complemented with the pRARE2 plasmid (Novagen) was transformed with pnEA-3CH:His6-*SNU13* plasmid [25]. The recombinant His6-Snu13p was expressed in 1 L Luria Bertani medium, overnight at 20 °C after induction with 0.2 mM IPTG when OD_{600} reaches 0.6–0.8. The ^{15}N labeled protein was produced in M9 minimal medium supplemented by 0.5 g L^{-1} of $^{15}NH_4Cl$. The cells were harvested at 8 000 rpm (Beckman Coulter Avanti JXN-26 centrifuge, JLA-8.1000 rotor) for 15 min at 10 °C and the pellet resuspended in 30 mL of lysis buffer (HEPES-KOH 25 mM pH 7.5; NaCl 300 mM; imidazole 10 mM; TCEP 0.5 mM), sonicated and centrifuged at 20 000 rpm (Beckman Coulter Avanti J-20XP centrifuge, JA-20 rotor) for 30 min at 4 °C. Supernatant was incubated with 0.0125% PEI for 15 min at 4 °C to precipitate nucleic acids, centrifuged again at 20 000 rpm for 20 min at 4 °C, filtered on a 0.45 μm filter and purified on affinity resin (Talon® Superflow Metal Affinity Resin, Clontech). The protein without the His6-tag was collected after overnight cleavage by PreScission protease (in-house) on the beads, concentrated and purified on a gel filtration column (HiLoad® 16/600 Superdex® 75 pg , GE Healthcare) in 50 mM sodium phosphate buffer (pH 6.4) and 100 mM NaCl. The protein from the elution peak was used to perform ITC experiments and NMR titrations.

2.3. NMR spectroscopy

NMR experiments were recorded at 500 and 600 MHz on an Avance NEO and Avance III Bruker spectrometers equipped with a z-gradient TBI probe (at 500 MHz) and a z-gradient TXI cryoprobe (at 600 MHz). NMR data were processed using TopSpin (Bruker) and analyzed with NMRFAM-SPARKY software packages [26]. NMR experiments were performed in 50 mM sodium phosphate buffer (pH 6.4) and 100 mM NaCl. The concentration of unlabeled and labeled RNA samples ranged from 0.2 to 0.8 mM. Sample volumes were 150 μL in 3 mm NMR tubes.

^{1}H, ^{13}C, ^{15}N and ^{31}P assignments were obtained using standard homonuclear and heteronuclear methods. NMR data were acquired at 10 °C, 15 °C and 25 °C for exchangeable protons and at 15 °C, 20 °C, 25 °C and 30 °C for non-exchangeable protons. Solvent suppression for samples in 90%/10% H_2O/D_2O was achieved using combined "Jump and Return" and WATERGATE sequences [27–29]. The residual HDO resonance in 99.9% D_2O was suppressed using low power presaturation. Two-dimensional NOESY spectra in 90%/10% H_2O/D_2O were acquired with mixing time of 50 ms, 70 ms, 150 ms, 300 ms and 400 ms. Base-pairing was established via sequential Nuclear Overhauser Effects (NOEs) observed in 2D NOESY spectra at different mixing times and directly observed from J(N,N)-HNN COSY experiments performed in 90%/10% H_2O/D_2O at 15 °C and 25 °C [30,31]. NOESY spectra with mixing times of 50, 150 and 400 ms in 99.9% D_2O were acquired at 20 °C, 25 °C and 30 °C.

Heteronuclear NMR spectra were measured at 25 °C in 99.9% D_2O with the exception of ^{1}H-^{15}N HSQC experiments that were acquired at 15 °C and 25 °C in 90%/10% H_2O/D_2O. ^{13}C and/or ^{15}N decoupling during acquisition was achieved using the GARP composite pulse sequence. Assignments of RNA were achieved using 2D NOESY experiments at different mixing times, 2D TOCSY and 2D COSY-DQF. Assignments of non-exchangeable protons of labeled RNA were completed using ^{1}H-^{13}C constant-time HSQC, 3D-HCCH-TOCSY, HCN and HCC experiments [32–35]. Dihedral restraints were obtained from HP-COSY and HCP experiments at 25 °C [36,37].

NOESY experiments recorded in 90%/10% H_2O/D_2O and in 99.9% D_2O, at different mixing times and various temperatures were also performed in the presence of 3 and 5 mM Mg^{2+}. Heteronuclear NMR spectra (^{1}H-^{15}N HSQC, ^{1}H-^{13}C HSQC) were also acquired with Mg^{2+} concentration ranging from 1 to 10 mM.

For residual dipolar coupling (RDC) experiments, partial alignment of $^{13}C/^{15}N$ labeled RNA was achieved by adding Pf1 filamentous bacteriophage supplied in 10 mM sodium phosphate buffer at pH 6.5 (ASLA Biotech Ltd), resulting in a splitting of the deuterium solvent line of 11 Hz. ^{1}H-^{15}N and ^{1}H-^{13}C residual dipolar couplings (RDCs) were calculated as the difference between couplings measured for isotropic and partially aligned samples with IPAP-HSQC and TROSY experiments recorded at 25 °C [38].

2.4. Distance and dihedral restraints for structure calculation

Distance restraints involving non-exchangeable protons were derived from cross-peak intensities in NOESY experiments at 25 °C, using the H5/H6 cross-peaks of pyrimidines as internal standard.

Inter-proton distances derived from NOE cross-peaks were classified into four distance bound ranges: strong (1.8–3.0 Å), medium (3.0–4.5 Å), weak (4.0–5.5 Å) and very weak (4.5–7.0 Å). Hydrogen bonding restraints were used for Watson-Crick base pairs from G1•C31 to C5•G27 and G12•C23 to C15•G20, and for G9•A26 and A10•G25 sheared base pairs. Classical A-helix values were used for stem residues: $\alpha = -65 \pm 30°$, $\beta = 178 \pm 30°$ and $\varepsilon = -155 \pm 30°$. For residues G6 to G12, U16 to G20 and U24 to G27, α was left unconstrained, As determined from analysis of $^{3}J_{P\text{-}H5'}$, $^{3}J_{P\text{-}H5''}$ and $^{3}J_{P\text{-}C4'}$ from HP-COSY and HCP experiments, β was constrained to the *trans* conformation ($178 \pm 30°$) for most residues, except for G6, A10, U11, G12, G19, A26 and G27 that were left unconstrained, ε was constrained to the *trans* conformation ($-155 \pm 30°$) for most of residues, with the exception of C5 and G6, G12, A25 and A26 that were left unconstrained, G7, U8, G9, U11, U17, C18 and U24 that were constrained to *gauche*$^-$ conformation ($260 \pm 30°$) as determined from the analysis of $^{3}J_{H3'\text{-}P}$, $^{3}J_{C2'\text{-}P}$ and $^{3}J_{C4'\text{-}P}$ derived from HP-COSY and HCP experiments. Torsion angles χ were derived from the observation of intra-residue H6/H8-H1′ cross-peak volumes. All bases were restrained to anti-conformation ($-158 \pm 30°$), with the exception of G7 and U11, which χ angles were loosely constrained, and U8, G9, U17, C18, G25 and A26 which χ angles were constrained to a *syn* conformation ($-136 \pm 30°$). The ribose sugar pucker was determined from analysis of H1′-H2′ coupling constants. Torsion angles ν_0 to ν_4 were derived from the analysis of COSY-DQF and TOCSY experiments. Nucleotides with no COSY and no TOCSY cross-peaks between H1′ and H2′ protons were restrained to the *C3′-endo* conformation ($\nu_0 = 6 \pm 15°$, $\nu_1 = -25 \pm 15°$, $\nu_2 = 37 \pm 15°$, $\nu_3 = -37 \pm 15°$, $\nu_4 = 21 \pm 15°$). Nucleotides G7, U8, G9, A10, U17, C18, G25 and A26 with cross-peaks in TOCSY and COSY spectra were classified as *C2′-endo* ($\nu_0 = -21 \pm 20°$, $\nu_1 = 35 \pm 20°$, $\nu_2 = -35 \pm 20°$, $\nu_3 = 24 \pm 20°$, $\nu_4 = -2 \pm 20°$).

2.5. Structure calculations

Structures were calculated with CNS (Crystallography and NMR System) torsion angle molecular dynamics (TAMD) protocol for nucleic acids using NOE and dihedral angle restraints [39]. One hundred structures were generated from a randomized extended strand. The first stage consisted of a high-temperature torsion angle dynamics for 30 ps at 20 000 K with a van der Waals scale factor of 0.1. During the second stage, the molecules were cooled for 40 ps of torsion angle dynamics with a van der Waals scale factor increased from 0.1 to 1. In the third stage, molecules were submitted to a second slow cooling for 35 ps in Cartesian space where the van der Waals scale factor increased from 1 to 4. Finally, 10 Powell cycles of energy minimization of 300 steps each were done.

In a second step, the structures were refined by adding RDC data to the structural restraints. Axial (Da) and rhombic (R) components of the aligned tensor were determined from structures calculated in the absence of RDCs with zero violation on NOE distance (0.2 Å) and dihedral angle (5°). The initial alignment tensor was first estimated from the best fit of observed RDCs to the calculated prefolded structures, using PALES software [40]. An extensive grid search was then used to determine optimal Da and R values which were calculated at −12.5 Hz and 0.45, respectively [41]. The prefolded structures were next submitted to a calculation including RDC data. The first stage consisted of a torsion angle dynamics for 10 ps at 300 K with a van der Waals scale factor of 0.1. During the second stage, the molecules were cooled for 9 ps of torsion angle dynamics with a van der Waals scale factor increased from 0.1 to 1. The SANI force constraint used for RDCs was gradually increased from 0.01 kcal mol^{-1} Hz^{-2} to 1.00 kcal mol^{-1} Hz^{-2}. Finally, 10 Powell cycles of energy minimization of 800 steps each were done. These structures, with no violation and the best fit with RDC data, were further refined using the nucleic acid force field to include optimized potentials for liquid simulation (opls), charges and non-bonded parameters [42]. Quality factors (Q) and root-mean-square deviations (r.m.s) between input and calculated RDCs were calculated with the PALES software for the 10 final converged structures [43] (Table 1, Supplementary Table 1 and Supplementary Fig. 2). Structures were visualized and analyzed with Pymol and 3DNA software packages [44,45].

2.6. NMR titration experiments

All titrations experiments were performed at 25 °C. Complexes were formed by addition of protein to both unlabeled and $^{13}C/^{15}N$ labeled kt-U14 monitoring the imino protons region of 1D spectra and $^{1}H\text{-}^{15}N$ HSQC, respectively. Complexes were also formed by stepwise addition of kt-U14 to protein monitoring the amide region of $^{1}H\text{-}^{15}N$ HSQC spectra. ^{15}N decoupling during acquisition time was achieved using GARP composite pulse sequence.

2.7. Isothermal titration calorimetry

ITC experiments were performed using an ITC-200 microcalorimeter (GE Healthcare). U14 RNA was synthesized using T7 RNA polymerase as described above and extensively dialyzed against the buffer used for ITC experiments. RNA sample was refolded by heating at 95 °C (2 min) and snap-cooled at 4 °C. The protein Snu13 was expressed and purified as described above. The concentrations of RNA sample in the cell and Snu13p in the syringe were 58 μM and 818 μM respectively. Titration experiments were performed at 30 °C in 50 mM sodium phosphate buffer (pH 6.4) and 100 mM

Table 1
NMR restraints and statistics for the 10 converged structures.

Distance and dihedral restraints	
Intra-residue distance restraints	299
Inter-residue distance restraints	243
Hydrogen bonding distance restraints	66
Total distance restraints	608
Torsion angle restraints for sugar pucker	150
Backbone angle restraints	91
Total angle restraints	241
Total restraints	849
Residual Dipolar Couplings	37
r.m.s. deviation from experimental restraints	
Distance restraints (Å)	0.0565 ± 0.0012
Dihedral restraints (°)	0.4929 ± 0.0037
Deviation from idealized geometry	
Bond (Å)	0.00583 ± 0.00004
Angle (°)	0.9852 ± 0.0068
Impropers (°)	0.6598 ± 0.0045
r.m.s.d.[a] (Å)	
All atom	0.61 ± 0.04
Heavy atom	0.56 ± 0.04
Backbone	0.58 ± 0.04
RDCs quality [b]	
Q [c]	0.0777 ± 0.0006
r.m.s. ($^{1}D_{NH}$) (Hz) [d]	0.297 ± 0.009
r.m.s. ($^{1}D_{CH}$) (Hz) [d]	0.792 ± 0.022

[a] Root mean square deviation ± SD compared to the global average structure for all structures.

[b] Quality of residual dipolar couplings (RDCs) data calculated with the PALES software [43] reported after refinement with the nucleic acid force field to include optimized potentials for liquid simulation (opls), charges and non-bonded parameters [42].

[c] Q: RDC Q-factor calculated according to $Q = \{\Sigma_{i=1,..,N}[d_i^{norm}(exp) - d_i^{norm}(calc)]^2/N\}^{1/2}/D^{r.m.s}$, with N being the number and measured and normalized couplings, $d_i^{norm}(exp)$. $D^{r.m.s}$. refers to root-mean-square value of RDCs for randomly distributed inter-nuclear vectors. Calculations of Q factors include both $^{1}H\text{-}^{15}N$ and $^{1}H\text{-}^{13}C$ RDCs.

[d] r.m.s: root-mean-square deviation between input and calculated RDCs.

NaCl, under constant stirring at 750 rpm, with 25 × 1.5 μL injections into 200 μL sample cell volume, with 3 min between injections.

Calorimetric data were first treated with NITPIC1.0.0a [46] then analyzed with Origin7 (GE-Healthcare).

2.8. EMSA experiments

Yeast full-length U14 box C/D snoRNA was synthesized by *in vitro* transcription with T7 RNA polymerase using as template a PCR fragment carrying the *S. cerevisiae* snoRNA coding sequence. After transcription, the RNA was dephosphorylated by treatment with the Calf Intestinal Phosphatase and 5′-end labeled with the T4 polynucleotide kinase in presence of [γ-^{32}P] ATP. For electrophoresis mobility shift assays (EMSA), 5 fmol of ^{32}P-radiolabeled U14 RNA (500 cpm) were mixed with increasing amount of recombinant Snu13p in 10 μL of buffer D (20 mM HEPES-KOH, pH 7.9; 150 mM KCl; 1.5 mM $MgCl_2$; 0.2 mM EDTA; 10% glycerol). After incubation 20 min on ice, the RNA–protein complexes formed were resolved by native gel electrophoresis at 4 °C.

3. Results and discussion

3.1. Resonance assignment of kt-U14

To identify the conformation adopted by the free C/D box snoRNA U14 recognized by Snu13p, we set out to determine the solution structure of the 31 nucleotides RNA (Fig. 1B and C). A thermo-stable UUCG tetraloop, followed by a C:G base pair on its 5' side, was added to ensure proper folding of the RNA (Fig. 1C) [47,48]. The terminal A:U and U:A base pairs present in the full-length RNA were substituted with two G:C base pairs to improve transcription yield (Fig. 1B and C).

The secondary structure was characterized by the analysis of 2D NOESY and ^{1}H-^{15}N HSQC experiments recorded in 90%/10% H_2O/D_2O at various temperatures (see Materials and Methods section; Fig. 2, top). Watson-Crick ^{15}N-H-^{15}N hydrogen bonds were directly observed in heteronuclear J(N,N)-HNN COSY experiments performed in H_2O [30,31]. The imino proton chemical shifts of the UUCG tetraloop are known and were used as a starting point for imino protons assignment located in the NC stem [49]. The resonances at 13.5 ppm and 14.1 ppm were assigned to U28-H3 and U22-H3, respectively, further allowing the identification of remaining imino protons in C and NC stems. As shown in Fig. 2 (top), in the region between 12 and 14 ppm, smaller resonances arising from a second minor form are observable (indicated by a star). Analysis of NOESY experiments did not allow its unambiguous characterization. Finally, NMR spectra display broad resonances between 9 and 12 ppm. Resonances at 9.4 ppm and 10.4 ppm were assigned to G9-H1 and G25-H1, respectively, from analysis of NOESY spectra recorded at 10 °C. G9-H1 gives rise to NOE cross-peaks with G9-H1' and A26-H8 while G25-H1 shows a correlation with U24-H5 (Supplementary Fig. 1; discussed below). Interestingly, the NH resonances of G9 and G25 are broad but observable, at expected chemical shifts as previously reported

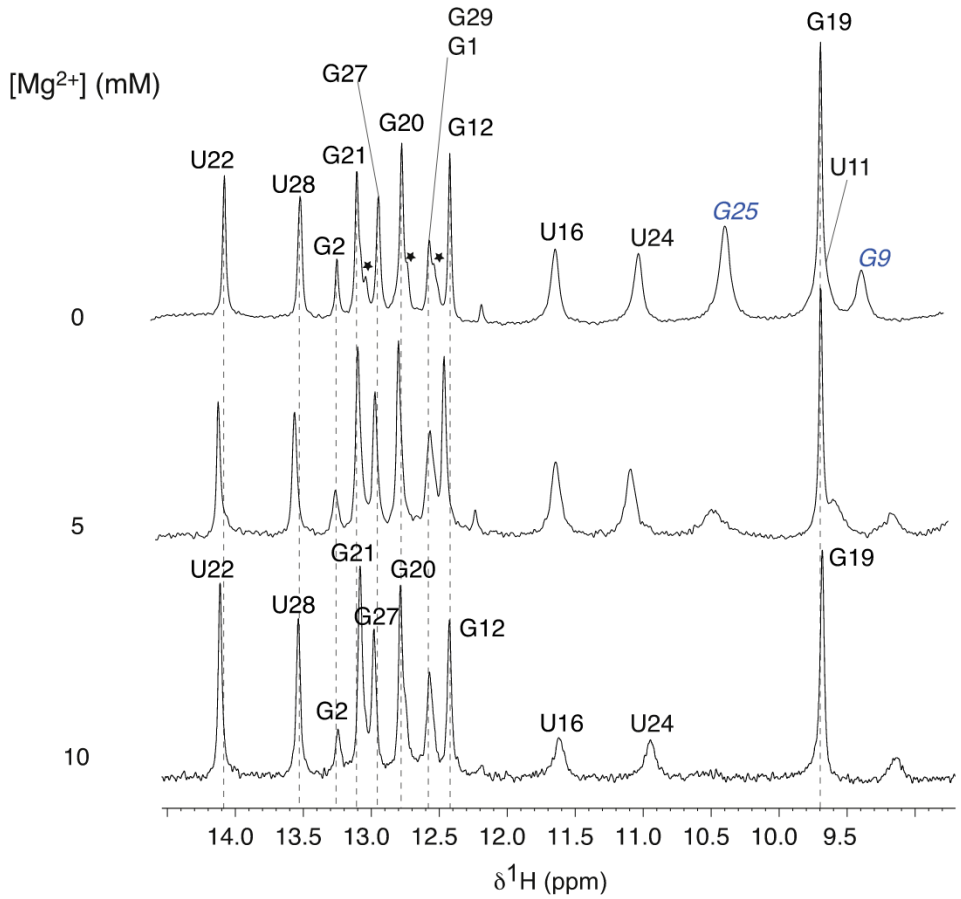

Fig. 2. The U14 snoRNA adopts a major expected conformation in equilibrium with a minor form disappearing upon magnesium addition. Imino protons region of 1D spectra recorded at 15 °C in 50 mM phosphate buffer (pH 6.4) with 100 mM NaCl, in the absence of magnesium (top), in the presence of 5 mM Mg^{2+} (middle) and 10 mM Mg^{2+} (bottom). All imino protons were assigned via sequential Nuclear Overhauser Effects (NOEs) observed in 2D-NOESY experiments. Imino protons of the UUCG apical loop which ensures a proper folding of the RNA, resonate at the expected chemical shifts typically observed [47,48].

[50–53]. Similarly, resonances at 9.6 ppm, 11.0 ppm and 11.7 ppm could be assigned to U11, U24 and U16 respectively. U24 imino proton exhibits weak connectivities with G12-H1 and U11-H3 (Supplementary Fig. 1).

Assignment of non-exchangeable protons and their directly bound carbons and nitrogens were obtained using standard homonuclear and heteronuclear 2D and 3D correlation experiments (^{1}H, ^{15}N, ^{13}C, ^{31}P) [32–34,36,37]. It is worth noting that the minor form present in solution gave rise to a little number of weak independent NOE cross-peaks that did not interfere with NOE correlations related to the major conformation. For this latter major form, sequential H6/8-H1' connectivities observed in a classical helix A were identified for all residues, except for G7, U8, G9, A10, G25, A26 and the apical loop (described in section 3.2).

3.2. Three-dimensional structure of U14 snoRNA major conformation

The three-dimensional structure of U14 snoRNA was determined using distance and dihedral torsion restraints and residual dipolar coupling constants (RDCs) derived from NMR data recorded at 25 °C [38]. Structures were calculated using 608 NOE distance restraints, 241 dihedral torsion restraints and 37 residual dipolar coupling (RDC) constraints (Table 1 and Supplementary Table 1). The overall structure is well-defined with a root-mean-square deviation compared to the global average structure (r.m.s.d.) of 0.56 ± 0.04 Å (Table 1, Fig. 3). Back-calculated RDCs for the final 10 converged structures with the PALES software [43] show an excellent agreement with the predicted values (Supplementary Table 1 and Supplementary Fig. 2). The U14 snoRNA contains two helical A-type segments, the C and NC stems and displays a kinked shape of the phosphodiester backbone at the U8 nucleotide (apex of the curvature), with a φ angle value of 27.7 ± 0.6° (Fig. 3).

3.2.1. The internal loop adopts a conformation that slightly differs from known K-turns

G6, G7 and U8 residues are not stacked continuously. G6 is in a *C3′-exo* and *anti* conformations as analyzed by the 3DNA software [45]. Sequential H8-H1′ connectivity was observed with C5, as well as several NOE contacts between G6-H8 and C5-H6, -H2′ and -H3′, respectively. The G6 residue is stacked against the closing base pair of the C-stem as it has been observed in other free RNA K-turns such as U4 snRNA or *B. subtilis tyrS* T-box Leader RNA [53,54]. Analysis of converged structures revealed that G6 could be stabilized by a hydrogen bond involving G6(N2) and A26(O2′) which average distance is 3.49 ± 0.06 Å, consistent with a water mediated

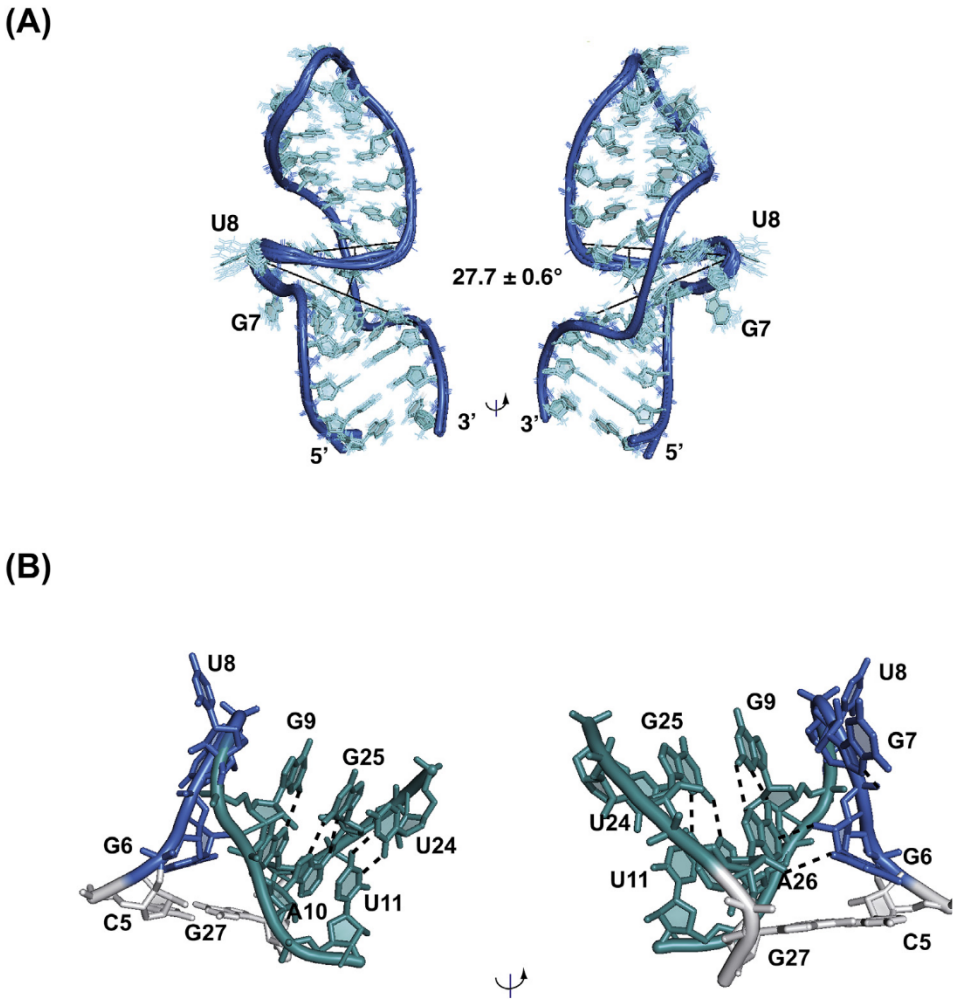

Fig. 3. Three-dimensional structure of U14 snoRNA. **(A)** Superimposition of 10 converged NMR structures. Bases and sugars are shown in light blue and the backbone in dark blue. The bend between NC and C stems was calculated from the angle between the P nuclei of G12, U8 and G29 residues [54,80]. Structures were analyzed using PyMol and 3DNA softwares [44,45]. **(B)** View of the internal loop. Broken lines indicate possible hydrogen bonds. Residues from the C-stem are shown in grey. The three nucleotides bulged G6, G7 and U8 are highlighted in dark blue. The NC-stem is shown in turquoise blue.

hydrogen-bond (Fig. 3). G7 is outside and devoid of stacking interaction. A weak H8-H1′ connectivity with G6 was observed. The G7-H1′ is shifted upfield to around 4.77 ppm, indicative of a conformation that deviates from standard stacking (Supplementary Fig. 3). The H1′/H2′ cross-peak observable in COSY and TOCSY experiments indicated a *C2′-endo* conformation of G7 sugar pucker, whereas β and ε were constrained to *trans* and *gauche*$^-$ conformations respectively, as determined from analysis of HP-COSY and HCP experiments. In the structures, the average distance between G7(N7) and G7(O2P) is 3.4 ± 0.1 Å which is compatible with a water mediated hydrogen bond that could contribute to the stabilization of G7. Finally, U8 is swung outside adopting a *C2′-endo* and *syn* conformations with β and ε torsion angles in *trans* and *gauche*$^-$ conformations (Fig. 3). Only two inter-residue contacts involving U8-H6 and G7-H4′, U8-H2′ and G7-H4′ could be detected. U8 is fully exposed to solvent and consequently provides an anchor for Snu13p interaction. Interestingly, the substitution of this uridine by another nucleotide completely abolishes the interaction with the human protein [55]. In previous works, the binding of L7Ae-like proteins has been described to open up the major groove of the RNA exposing mainly the major groove edges of the conserved guanine bases of the G•A pairs and projected out the third base of the bulge (N_3) [2]. In the case of kt-U14, the uridine is already outside before the arrival of the protein which suggests a different mechanism of recognition, contrasting with the U4 snRNA in which the corresponding U is weakly stacked on the preceding A nucleotide (position N_2).

3.2.2. *U11•U24 forms an asymmetric base pair*

Nucleotides U11 and U24 are stacked at the 3′ side of the NC stem in *C3′-endo* and *anti* conformations with ε constrained to *gauche*$^-$ conformations, as determined by NMR experiments. U11 and U24 display broad imino protons indicative of weak hydrogen bonds (Fig. 2). Nevertheless, several NOE contacts and dihedral restraints, extracted from non-exchangeable proton NMR data, place U11 and U24 unambiguously stacked inside. Sequential H8/6-H1′ connectivities were observed between G12 and U11, and U24 and C23. In addition, U11-H1′ and U24-H2′ exhibit upfield chemical shifts at 4.61 and 3.62 ppm respectively, as similarly observed in the case of *B. subtilis tyrS* T-box Leader RNA (Supplementary Fig. 3) [53]. Finally, the hydrogen bond pattern was established using chemical shift data [53]. A 2D HCC experiment that shows pyrimidine H5-C4 correlations, pointed out that U24-C4 is shifted upfield while U11-C4 exhibits an usual chemical shift (Fig. 4) [35]. These data support that U11•U24 forms an asymmetric base pair with the hydrogen bond pattern U11(H3)-U24(O2) and U11(O4)-U24(H3) [53].

3.2.3. *A tandem sheared G•A base pairs is formed through a weak hydrogen bonds network*

Several NOE contacts positioned G9, A10, G25 and A26 stacked inside in *C2′ endo* and *anti* conformations, except for A10 which is in *C1′ exo* conformation. NMR data sustain the existence of the tandem sheared G•A base pairs. First, as mentioned above, G9-H1 and G25-H1 are observable at expected chemical shifts, as it has been previously described for G•A sheared base pairs [50–53]. As measurable in the ensemble of structures, G25-H1 could be involved in water-mediated hydrogen bond with G9-O2′ (average distance: 4.6 ± 0.1 Å). Surprisingly, G9-H1 is visible although it is not involved in hydrogen bonding, which is reminiscent with the observation made in the free U4 RNA [54]. HNN experiments failed to provide direct evidence of the formation of the sheared G•A base pairs, which is consistent with a weak hydrogen bond network as previously reported [53]. However, analysis of the first converged structures with no hydrogen bond constraints for G9•A26 and A10•G25 revealed that they adopt a G•A sheared base pair conformation.

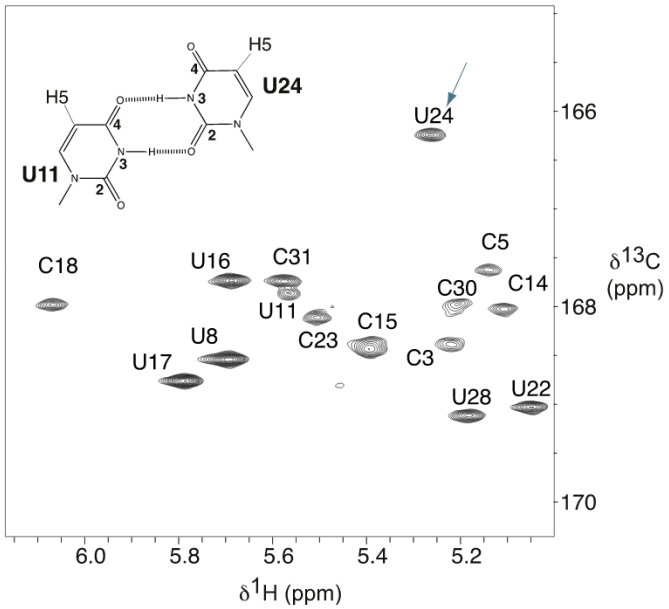

Fig. 4. U11•U24 forms an asymmetric base pair with the hydrogen bond pattern U11(H3)-U24(O2) and U11(O4)-U24(H3). ^{1}H-^{13}C HCC experiment was recorded at 25 °C in 50 mM sodium phosphate buffer and 100 mM NaCl. H5-C4 correlations are observable for pyrimidine residues [35]. H5 protons assignments were achieved from analysis of NOESY and MLEV experiments recorded in the same conditions. The residue U24-C4, highlighted with an arrow, exhibits an upfield chemical shift in comparison to other U-C4.

Hydrogen bonds were consequently progressively added during the calculation. In addition, unusual chemical shifts and NOE cross-peaks characteristics of this motif are observable. Indeed, the H1′ resonance of the residue 3′ to the A involved in a sheared G•A base pair has been reported to exhibit an upfield chemical shift, as seen for U11-H1′ stacked against the sheared A10•G25 (Supplementary Fig. 3) [56]. In addition, U24-H2′ and A26-H2′ are shifted upfield at 3.62 and 4.95 ppm respectively, while A26-H1′, G9-H2′ and G25-H2′ are shifted downfield at 6.34, 5.07 and 4.95 ppm, respectively (Supplementary Fig. 3). Similar chemical shifts have been reported in the *B. subtilis tyrS* T-box Leader RNA [53]. Strong cross-strand NOEs corresponding to a distance shorter than 3.5 Å are observable between A26-H2 and G6-H1′, and A26-H2 and A10-H1′ (Fig. 5). In the final ensemble of 10 structures, the corresponding distances are 2.9 ± 0.1 Å and 2.8 ± 0.1 Å, respectively (Table 2). Notably, as shown in Table 2, such spectral signature would not be observed in a more extended conformation as observed for kt-U4 (Fig. 6). Less intense cross-strand NOEs involving the following atom pairs A26-H1′/G27-H1′ and A26-H1′/A10-H1′ were also identified (Fig. 5). The corresponding distances in the ensemble of structures are 3.1 ± 0.1 Å and 4.6 ± 0.1 Å, respectively (Table 2). Analysis of structures also shows that G9 and G25 are involved in a base-stacking interaction together, as well as A10 and A26 (Fig. 3). Finally, the typical predicted hydrogen bond found in K-turn motif, between the 2′-OH of the position *1* and the N1 of position *7* (Fig. 1A), is observed for G6 and A26 residues (Fig. 3) [52]. The measured distance between A26-N1 and G6-O2′ is 2.9 ± 0.1 Å in the ensemble of structures, which is compatible with the formation of a direct hydrogen bond (Fig. 4). Notably, this K-turn signature is not visible in the U4 snRNA structure where the corresponding distance is measured at 4.8 ± 0.1 Å. All these observations sustain that U14 adopts a major conformation close to bound RNA K-turn but with a weak hydrogen bond pattern. The φ angle between C- and NC-stems in U14, which value is 27.7 ± 0.6°, is similar to angles observed in bound U3 B/C box and archaeal C/D box RNP (Fig. 6). Unbound U4 and *tyrS* RNAs

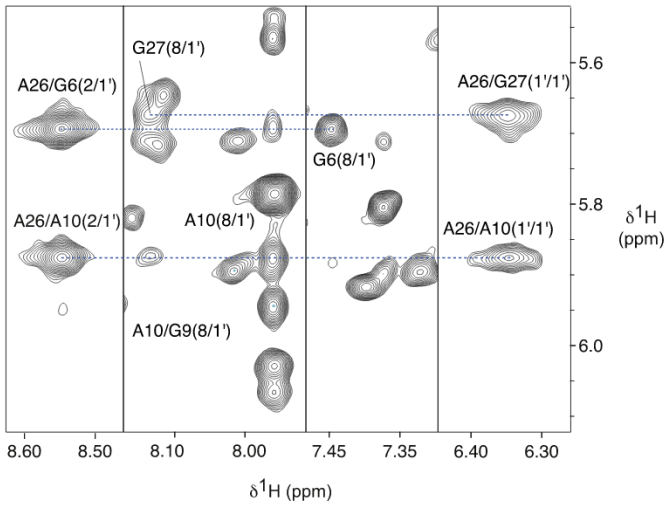

Fig. 5. NOE characteristics of a K-turn structure. Zooms of 2D NOESY spectra recorded at 25 °C, with a mixing time of 400 ms, in 50 mM sodium phosphate buffer (pH 6.4) with 100 mM NaCl in 99.9% D_2O. NOE features of the K-turn structure are indicated with broken lines.

exhibit larger φ angles values which are respectively 70.4 ± 1.7° and 67.5 ± 0.6°, corresponding to more extended conformations. These K-turns will be unfolded up to the partner is bound, a classic example of induced fit. It has been reported that a free RNA containing a K-turn sequence could be effectively subjected to a dynamic exchange with two-state equilibrium between a tightly kinked K-turn structure or a more relaxed form typical of any three-base bulge with a different relative proportion depending on the type of K-turns and the chemical environment [57]. By contrast, U14 is already pre-folded in a K-turn structure dominated by a weak hydrogen bond network, thus favouring the interaction with Snu13 core protein. It has been effectively reported that the recombinant human SNU13 protein displays a better affinity for the U14 snoRNA. Watkins and collaborators performed gel mobility shift assays of U3, U14 snoRNAs and U4 snRNA with increasing concentrations of recombinant human SNU13 protein to obtain apparent K_D of 30, 8 and 20 nM respectively [3]. In any case, k-turns function as an RNA-protein platform to generate large RNPs in cellular context.

3.3. Effect of magnesium on U14 structure

Since Mg^{2+} ions are involved in RNA folding, we examined its impact on U14 structure. NMR titrations monitoring exchangeable, aromatic and sugar protons were performed to detect potential Mg^{2+} binding sites by chemical shift perturbation analysis. As shown in Fig. 2, slight NH chemical shifts variations are observable upon magnesium addition, with the exception of G25-H1 that undergoes broadening. Interestingly, NH resonances arising from the minor form present in solution disappeared with increasing concentration of magnesium. H5-H6 cross-peaks in MLEV experiment also pointed out that the weaker supplementary correlations arising from the minor form undergo broadening upon magnesium addition (Supplementary Fig. 4). U-H6 and C-H6 chemical shifts variations are generally limited to less than 0.07 ppm. C8-H8, C2-H2 and C1′-H1′ cross-peaks undergo chemical shift changes limited to less than 0.15 ppm for both ^{13}C and ^{1}H (Supplementary Fig. 5).

Our NMR results indicate that magnesium addition did not induce significant changes in spectra, with the exception of broadening of the resonances arising from the minor fraction (Fig. 2 and Supplementary Figs. 4 and 5). Previous studies have demonstrated that the K-turn motif can exist in linear and bent conformations and that this equilibrium can be displaced upon Mg^{2+} binding [58–60]. Unfortunately, our data did not allow the characterization of the minor form of U14. Although this latter is not visible, we cannot exclude that this second conformation is still present in solution.

3.4. Interaction with Snu13p

We first examined the interaction of Snu13p with U14 snoRNA in the wider context of the full-length RNA using EMSA experiments. The RNA binds the protein and caused a band shift variation that increased with increasing amounts of Snu13p (Fig. 7A). The apparent K_D value was estimated at 0.1 μM. We next used ITC to more accurately determine the affinity between our NMR construct and the protein (Fig. 7B). The affinity of Snu13p for kt-U14 was calculated to have a K_D value of 0.15 ± 0.06 μM, which is in good agreement with the value measured by EMSA experiment with the full-length RNA.

NMR was then used to structurally investigate Snu13p binding to kt-U14 RNA. Chemical shift perturbations of imino protons were first monitored upon protein binding. Unlabeled Snu13p addition induced several changes in the imino proton region (Fig. 8A). Imino protons in the Snu13p:RNA complex were assigned from the analysis of 2D NOESY and ^{1}H-^{15}N HSQC experiments, with the exception of G9-H1 and G25-H1 that could not be unambiguously discriminated at 10.2 and 11.5 ppm, and new resonances between 11.34 and 11.67 ppm (Fig. 8A). Notably, resonances arising from the minor form disappeared during the complex formation. Interestingly, previous real-time binding experiments established a passive model of conformational selection in which the protein selects an already folded RNA fraction, then resulting in equilibrium shift towards this form [61]. Imino protons from C- and NC- stems are slightly shifted (less than 0.09 ppm) which correlates with intermolecular contacts already described between the C-terminus α2 helix of Snu13p and the phosphate backbone [2]. G12-H1 and G27-H1 are shifted downfield (0.12 ppm), and are more affected, as they are located at the junction of essential elements for protein recognition. Based on reported assignment of ^{15}N-labeled Snu13p (BMRB: 15412 [62]), NMR titration experiments by adding increasing amounts of unlabeled U14 to the ^{15}N-labeled Snu13p were also performed. The three-dimensional structure of the yeast Snu13p folds into a α-β-α sandwich which shows a perfect conservation with the structures of the L7Ae archaea protein [63–66]

Table 2
Summary of distances between atom pairs observed for U14 snoRNA from *S.cerevisiae* compared to classical K-turns. Residues located in the internal bulge are numbered according to Figs. 1 and 6. Standard deviations are indicated for structures determined by NMR.

Structure (PDB code)	7(H2)/1(H1′)	7(H2)/5(H1′)	7(H1′)/-2(H1′)	7(H1′)/5(H1′)
U14	2.9 ± 0.1 Å	2.8 ± 0.1 Å	3.1 ± 0.1 Å	4.6 ± 0.1 Å
2xeb (Spliceosomal U4)	5.0 ± 0.1 Å	5.1 ± 0.0 Å	3.8 ± 0.2 Å	9.1 ± 0.1 Å
2kzl (*B. subtilis*)	7.1 ± 0.1 Å	2.7 ± 0.2 Å	4.9 ± 0.1 Å	4.6 ± 0.0 Å
5jpq (90S pre-ribosome)	4.7 Å	4.3 Å	2.8 Å	4.1 Å
1rlg (*A. fulgidus*)	3.0 Å	2.8 Å	2.6 Å	4.2 Å

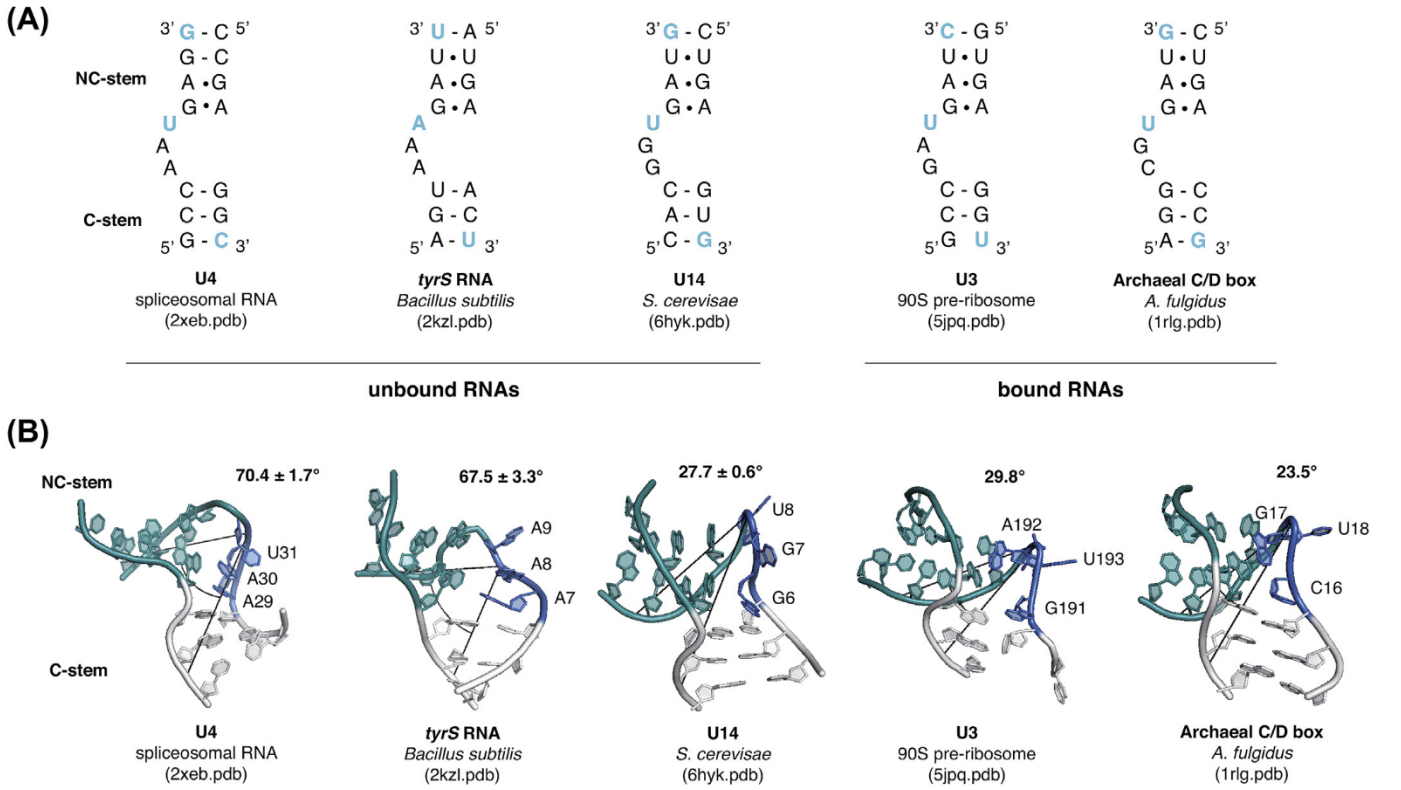

Fig. 6. Comparison of the free U14 structure with bound and unbound known K-turn motifs. The bend between NC- and C-stems is analyzed. **(A)** Sequences and secondary structures of several unbound and bound K-turns. **(B)** Angles φ between each stem are calculated from the angle between the P nuclei of nucleotides indicated in blue in the sequences, as previously described [54,80]. Residues from the C-stem are shown in grey. The three nucleotides bulged G6, G7 and U8 are highlighted in dark blue. The NC-stem is shown in turquoise blue.

(Fig. 7C; PDB Id: 2ALE). The E39 amino acid located in the α2 N-terminal of Snu13p described to make specific contacts with the conserved G•A pairs is shifted upon interaction with kt-U14, which correlates with the shift of G9 and G25 at 10.2 and 11.5 ppm (Figs. 7C, 8A and 8B). Snu13p has been also shown to recognize the N_2 and N_1 nucleobases of the bulge (G6 and G7 for kt-U14), essentially by covering them with a α4-β4 hydrophobic loop (motif VSRP) [2]. In addition, the pocket involving E59, R84, I63 and I98 is known to stabilize the protruding N_3-residue (U_3 for kt-C/D and kt-U4, U8 for kt-U14) [2,67]. The mutation of the E59 residue completely abolished the viability of the yeast cells [68]. Thus, the additional resonances between 11.34 and 11.67 ppm could correspond to imino protons from G6, G7 and U8 residues in the internal loop, which are known to be protected upon Snu13p binding. In our NMR experiments, E59, R84, I63 and I98 residues are effectively shifted upon interaction with kt-U14 (Figs. 7C and 8B).

NMR experiments pointed out that the binding of Snu13p to the pre-folded kt-U14 induces the strengthening of the hydrogen bond network, as clearly witnessed by the U11•U24 base pair, the enhancement of imino proton resonances intensities and the appearance of additional imino protons (Fig. 8A). Our results also show that the interaction occurs through the conserved reported interface of the protein. Further experiments will be necessary to establish the detailed and specific molecular principles of Snu13p binding to U14 snoRNA.

4. Conclusive remarks

In this work, we described the structure adopted by a major fraction of the kt-U14 RNA in the absence of protein and divalent ions. Our NMR studies reveal that free U14 RNA adopts a pre-folded conformation similar to known bound K-turn such as the one formed by the B/C motif in U3 snoRNA (kt-U3B/C) or in the archaeal C/D box. In contrast to these latter RNAs, the structure of the free kt-U14 is dominated by a weak hydrogen bond network in its central region. The sharp kink of the phosphodiester backbone observed differs from the structure of the free kt-U4 also obtained by NMR in comparable saline conditions. The bulged nucleotides are not stacked and the uridine is projected out providing a platform for protein interaction. This structure of U14 is the first example of a pre-formed K-turn C/D box snoRNA.

4.1. K-turn motifs of C/D box snoRNA family

Previous experiments of chemical and enzymatic modifications in solution showed that the naked kt-U4 and kt-U3 C'/D are in equilibrium between two more or less compact conformations of a preformed helix-loop-helix structure, and that Snu13p binding displaces the equilibrium toward the bound form of K-turn [13,69]. Interestingly, this helix-loop-helix structure does not pre-exist in the case of the naked kt-U3B/C, indicating that Snu13p can favour the RNA folding by induced-fit [13]. However, the kt-U3B/C sequence is highly conserved and Snu13p binding showed very little tolerance towards mutations, suggesting that a high selection pressure on the kt-U3B/C sequence could have been necessary to conserve the induced-fit upon Snu13p binding [13,70,71]. By contrast, the kt-U3C'/D, which is partially preformed, corresponds to a degenerated C/D motif and exhibits a very low affinity for Snu13p [13]. Recently, we have shown *in vitro* that this low affinity can be compensated, at least partially, by the assistance of the *trans*-acting factor Rsa1p [72]. Rsa1p is a central protein of a machinery dedicated to box C/D snoRNP assembly and it primarily

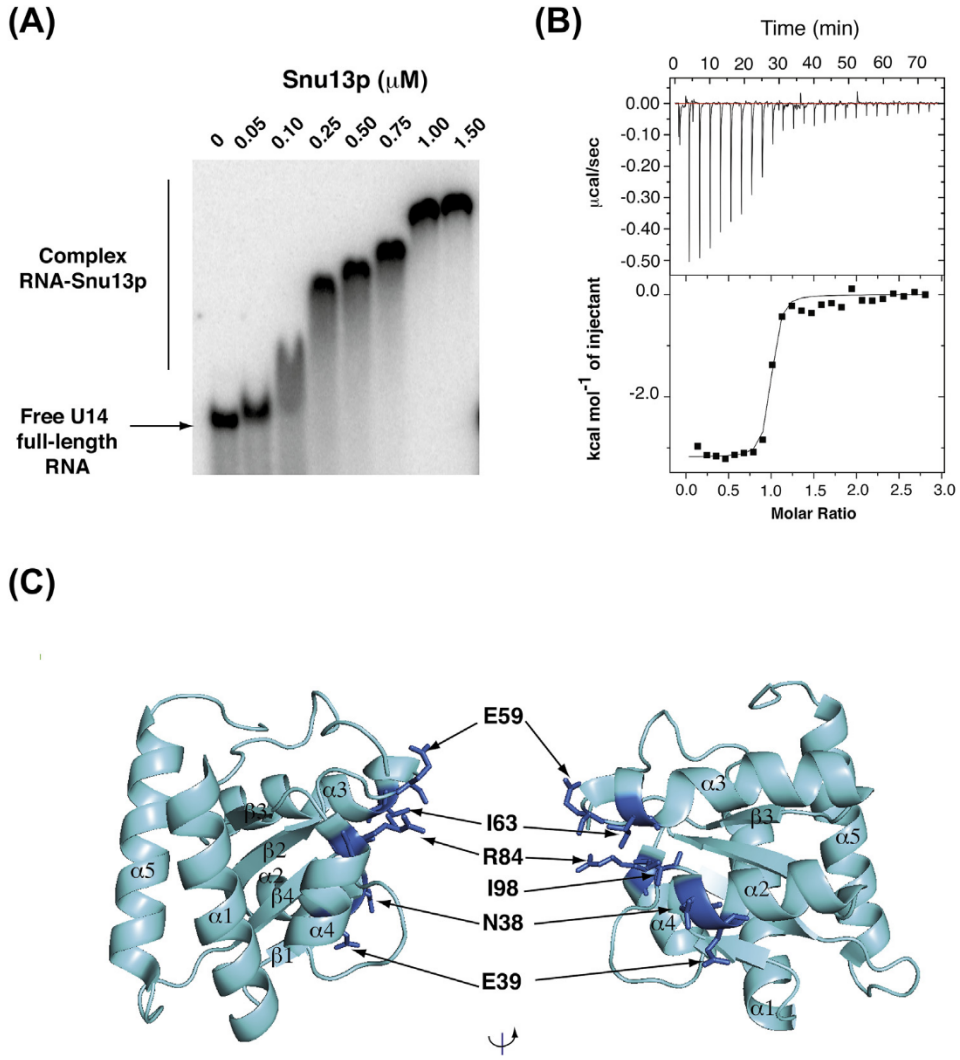

Fig. 7. Interaction with the Snu13 core protein. **(A)** Electrophoretic Mobility Shift Assays of full-length radioactively labeled U14 snoRNA at 0.5 nM with increasing concentration of the Snu13 core protein. **(B)** ITC experiment profile of the U14 (31-nt) titration by Snu13 protein. Raw data are shown on the top and integrated data on the bottom. **(C)** Three-dimensional structure of Snu13p using cartoon representation (PDB Id: 2ALE [66]). Residues cited in the text are highlighted.

binds to Snu13p [25,73,74]. Our data suggested that electrostatic contacts of Rsa1p with the RNA phosphate backbone may significantly increase the interaction surface between the protein subcomplex and the snoRNA to thermodynamically favour the U3 C′/D RNP formation [72]. Compared with these two well documented examples, the kt-U14 represents the first structural reference for the family of canonical C/D motifs and appears now as an additional paradigm, since it exhibits both, an optimal sequence and a pre-bound folded state that, combined together, likely explain its status of high-affinity binding site for Snu13p. By comparison with this canonical example, it will be interesting in the future to conduct structural investigations on non-canonical k-turns, such as poorly conserved C/D motifs or internal box C'/D' motifs. Indeed, the absence of some specific structural features could explain the requirement of an external scaffold, like Rsa1p, in order to preserve the assembly of entire and functional particles.

4.2. Genomic organization of snoRNP constituents and riboregulation

In contrast to its mammalian orthologue, yeast *U14* (or *SNR128*) gene is not intron encoded but located only 67 nucleotides downstream from another box C/D snoRNA gene, *SNR190* in dicistronic independent transcription unit [75]. Therefore, snR190 and U14 snoRNAs are co-transcribed as a bicistronic functional precursor which is processed by the RNA endonuclease Rnt1p to liberate individual mature transcripts. Unlike the U14 snoRNA, the snR190 snoRNA has not been shown as active for methylation. In this context, the presence of a kinked conformation in the U14 from the free state (unlike the other K-turns), may suggest a faster interaction kinetics with Snu13p. In addition, the identification of the precise sequences of the boxes C' and D' will allow their structural characterization (Fig. 1) [18]. It would be interesting to know the conformational type of this K-turn and its possible difference in kinetic and thermodynamic properties with C/D boxes could be essential for the snoRNP U14 assembly and its function.

The K-turn structures are present in the 5′-UTR of multiple genes encoding proteins required in snoRNP assembly. As examples, in archaea, L7Ae binds the mRNA of its own gene, folds the K-turn and stabilizes the stem-loop that would occlude the ribosome binding site, thus preventing translation [76]. In the mRNA of a dicistronic gene encoding box C/D proteins NOP5 and Fibrillarin and in the *CBF5* gene that encodes the pseudo-uridine synthase of the H/ACA snoRNP, putative k-turns have been identified [77]. In

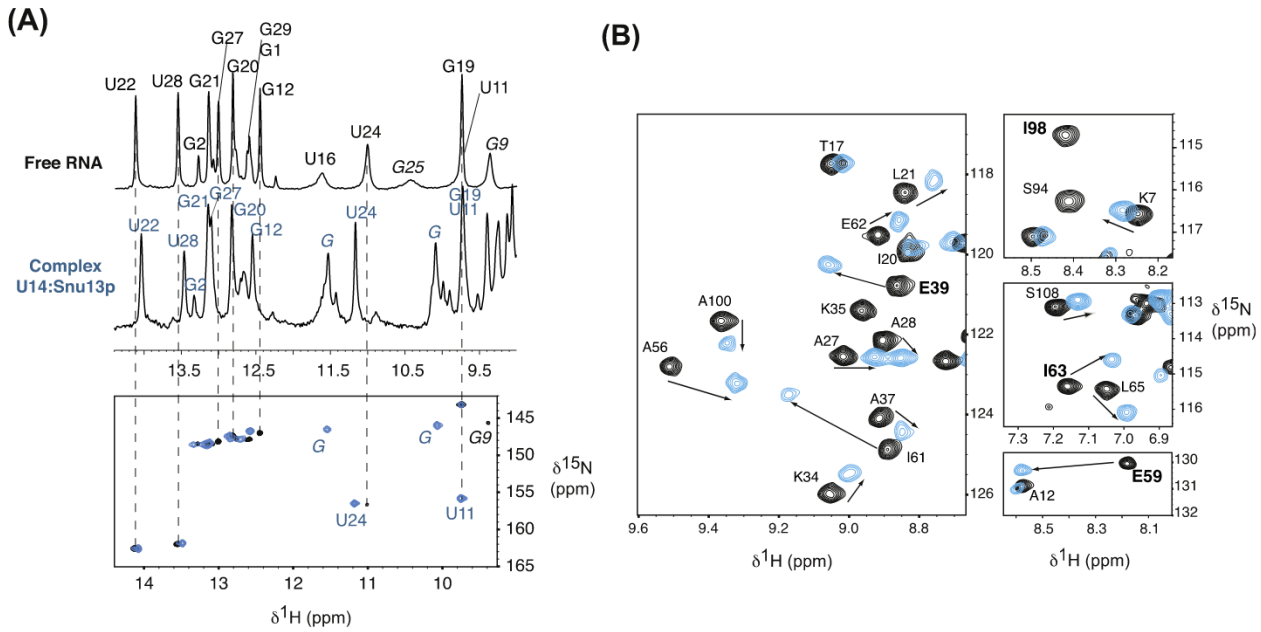

Fig. 8. Interaction between U14 RNA and the Snu13 core protein investigated by NMR. **(A)** Imino-proton region spectra recorded at 25 °C in 50 mM sodium phosphate buffer in 90%/10% H_2O/D_2O at pH 6.4, with 100 mM NaCl. The assignment of imino protons based on analysis of NOESY experiments is indicated for the free RNA (top, black) and the U14:Snu13p complex (middle, blue). On the bottom: overlay of ^{1}H-^{15}N HSQC spectra showing imino protons H1-N1 and H3-N3 of the free RNA (black) and the RNA in complex with Snu13p (blue). Tentative assignments are indicated in italic. **(B)** Overlay of ^{1}H-^{15}N HSQC spectra showing the free Snu13p (black) and in complex with kt-U14 (blue). Spectra were recorded at 25 °C in 50 mM sodium phosphate buffer at pH 6.4 and 100 mM NaCl. Residues from Snu13p that have been reported to make specific contact with RNA are highlighted in bold. Arrows indicate chemical shift changes upon binding. E39, E59 and I63 (left insets) undergo large chemical shifts variations upon binding to kt-U14. I98 disappears upon binding and could not be assigned in the complex.

human, some box C/D snoRNA k-turns are subject to probable regulation by N^6-methylation of one adenine of the sheared base pair (A_7, Fig. 1A) [78]. Indeed, this methylation negatively interferes directly with the interaction between SNU13 and box C/D and C'/D' k-turns. Altogether, these data suggest that the association between the SNU13/Snu13/L7Ae protein and k-turns is a keystone for controlling the assembly of many cellular RNPs and their downstream processes.

Coordinates

Atomic coordinates have been deposited in the Protein Data Bank (PDB ID code: 6HYK) and the NMR data in the Biological Magnetic Resonance Bank (BMRB access code: 34321).

Acknowledgments

This work was supported by Agence Nationale de la Recherche [Grant ANR-16-CE11-0032-02], CNRS, University of Lorraine, University of Strasbourg and INSERM. The authors thank the UMS 2008 for ITC and NMR facilities.

Appendix A. Supplementary data

Supplementary data to this article can be found online at https://doi.org/10.1016/j.biochi.2019.03.014.

References

[1] D.J. Klein, T.M. Schmeing, P.B. Moore, T.A. Steitz, The kink-turn: a new RNA secondary structure motif, EMBO J. 20 (2001) 4214–4221, https://doi.org/10.1093/emboj/20.15.4214.
[2] I. Vidovic, S. Nottrott, K. Hartmuth, R. Lührmann, R. Ficner, Crystal structure of the spliceosomal 15.5kD protein bound to a U4 snRNA fragment, Mol. Cell. 6 (2000) 1331–1342.
[3] N.J. Watkins, V. Ségault, B. Charpentier, S. Nottrott, P. Fabrizio, A. Bachi, M. Wilm, M. Rosbash, C. Branlant, R. Lührmann, A common core RNP structure shared between the small nucleoar box C/D RNPs and the spliceosomal U4 snRNP, Cell 103 (2000) 457–466.
[4] H. Mao, S.A. White, J.R. Williamson, A novel loop-loop recognition motif in the yeast ribosomal protein L30 autoregulatory RNA complex, Nat. Struct. Biol. 6 (1999) 1139–1147, https://doi.org/10.1038/70081.
[5] S.A. White, M. Hoeger, J.J. Schweppe, A. Shillingford, V. Shipilov, J. Zarutskie, Internal loop mutations in the ribosomal protein L30 binding site of the yeast L30 RNA transcript, RNA 10 (2004) 369–377.
[6] M. Daume, M. Uhl, R. Backofen, L. Randau, RIP-seq suggests translational regulation by L7Ae in archaea, MBio 8 (2017), https://doi.org/10.1128/mBio.00730-17.
[7] R.K. Montange, R.T. Batey, Structure of the S-adenosylmethionine riboswitch regulatory mRNA element, Nature 441 (2006) 1172–1175, https://doi.org/10.1038/nature04819.
[8] L. Huang, D.M.J. Lilley, The kink turn, a key architectural element in RNA structure, J. Mol. Biol. 428 (2016) 790–801, https://doi.org/10.1016/j.jmb.2015.09.026.
[9] P. Nissen, J.A. Ippolito, N. Ban, P.B. Moore, T.A. Steitz, RNA tertiary interactions in the large ribosomal subunit: the A-minor motif, Proc. Natl. Acad. Sci. U.S.A. 98 (2001) 4899–4903, https://doi.org/10.1073/pnas.081082398.
[10] Z. Kiss-László, Y. Henry, T. Kiss, Sequence and structural elements of methylation guide snoRNAs essential for site-specific ribose methylation of pre-rRNA, EMBO J. 17 (1998) 797–807, https://doi.org/10.1093/emboj/17.3.797.
[11] J.F. Kuhn, E.J. Tran, E.S. Maxwell, Archaeal ribosomal protein L7 is a functional homolog of the eukaryotic 15.5kD/Snu13p snoRNP core protein, Nucleic Acids Res. 30 (2002) 931–941.
[12] A.D. Omer, S. Ziesche, H. Ebhardt, P.P. Dennis, In vitro reconstitution and activity of a C/D box methylation guide ribonucleoprotein complex, Proc. Natl. Acad. Sci. U.S.A. 99 (2002) 5289–5294, https://doi.org/10.1073/pnas.082101999.
[13] N. Marmier-Gourrier, A. Cléry, V. Senty-Ségault, B. Charpentier, F. Schlotter, F. Leclerc, R. Fournier, C. Branlant, A structural, phylogenetic, and functional study of 15.5-kD/Snu13 protein binding on U3 small nucleolar RNA, RNA 9 (2003) 821–838.
[14] N.J. Watkins, A. Dickmanns, R. Lührmann, Conserved stem II of the box C/D motif is essential for nucleolar localization and is required, along with the 15.5K protein, for the hierarchical assembly of the box C/D snoRNP, Mol. Cell Biol. 22 (2002) 8342–8352.
[15] D.L. Lafontaine, D. Tollervey, Synthesis and assembly of the box C+D small nucleolar RNPs, Mol. Cell Biol. 20 (2000) 2650–2659.
[16] J.M. Hughes, M. Ares, Depletion of U3 small nucleolar RNA inhibits cleavage in

the 5' external transcribed spacer of yeast pre-ribosomal RNA and impairs formation of 18S ribosomal RNA, EMBO J. 10 (1991) 4231–4239.
[17] H.D. Li, J. Zagorski, M.J. Fournier, Depletion of U14 small nuclear RNA (snR128) disrupts production of 18S rRNA in Saccharomyces cerevisiae, Mol. Cell Biol. 10 (1990) 1145–1152.
[18] T. Dudnakova, H. Dunn-Davies, R. Peters, D. Tollervey, Mapping targets for small nucleolar RNAs in yeast, Wellcome Open Res 3 (2018) 120, https://doi.org/10.12688/wellcomeopenres.14735.1.
[19] A. Jarmolowski, J. Zagorski, H.V. Li, M.J. Fournier, Identification of essential elements in U14 RNA of Saccharomyces cerevisiae, EMBO J. 9 (1990) 4503–4509.
[20] J.P. Morrissey, D. Tollervey, U14 small nucleolar RNA makes multiple contacts with the pre-ribosomal RNA, Chromosoma 105 (1997) 515–522.
[21] D.A. Samarsky, G.S. Schneider, M.J. Fournier, An essential domain in Saccharomyces cerevisiae U14 snoRNA is absent in vertebrates, but conserved in other yeasts, Nucleic Acids Res. 24 (1996) 2059–2066.
[22] D.A. Dunbar, S.J. Baserga, The U14 snoRNA is required for 2'-O-methylation of the pre-18S rRNA in Xenopus oocytes, RNA 4 (1998) 195–204.
[23] J.F. Milligan, O.C. Uhlenbeck, Synthesis of small RNAs using T7 RNA polymerase, Methods Enzymol. 180 (1989) 51–62.
[24] J.R. Wyatt, M. Chastain, J.D. Puglisi, Synthesis and purification of large amounts of RNA oligonucleotides, Biotechniques 11 (1991) 764–769.
[25] B. Rothé, R. Back, M. Quinternet, J. Bizarro, M.-C. Robert, M. Blaud, C. Romier, X. Manival, B. Charpentier, E. Bertrand, C. Branlant, Characterization of the interaction between protein Snu13p/15.5K and the Rsa1p/NUFIP factor and demonstration of its functional importance for snoRNP assembly, Nucleic Acids Res. 42 (2014) 2015–2036, https://doi.org/10.1093/nar/gkt1091.
[26] W. Lee, M. Tonelli, J.L. Markley, Nmrfam-Sparky: Enhanced software for biomolecular NMR spectroscopy, Bioinformatics 31 (2015) 1325–1327, https://doi.org/10.1093/bioinformatics/btu830.
[27] M. Piotto, V. Saudek, V. Sklenár, Gradient-tailored excitation for single-quantum NMR spectroscopy of aqueous solutions, J. Biomol. NMR 2 (1992) 661–665.
[28] P. Plateau, M. Gueron, Exchangeable proton NMR without base-line distorsion, using new strong-pulse sequences, J. Am. Chem. Soc. 104 (1982) 7310–7311, https://doi.org/10.1021/ja00389a067.
[29] V. Sklenar, M. Piotto, R. Leppik, V. Saudek, Gradient-Tailored water suppression for 1H-15N HSQC experiments optimized to retain full sensitivity, J. Magn. Reson. Ser. A 102 (1993) 241–245, https://doi.org/10.1006/jmra.1993.1098.
[30] A.J. Dingley, S. Grzesiek, Direct observation of hydrogen bonds in nucleic acid base pairs by internucleotide $^{2}J_{NN}$ couplings, J. Am. Chem. Soc. 120 (1998) 8293–8297, https://doi.org/10.1021/ja981513x.
[31] M. Hennig, J.R. Williamson, Detection of N-H...N hydrogen bonding in RNA via scalar couplings in the absence of observable imino proton resonances, Nucleic Acids Res. 28 (2000) 1585–1593.
[32] R. Riek, K. Pervushin, C. Fernández, M. Kainosho, K. Wüthrich, [(13)C,(13)C]- and [(13)C,(1)H]-TROSY in a triple resonance experiment for ribose-base and intrabase correlations in nucleic acids, J. Am. Chem. Soc. 123 (2001) 658–664.
[33] J. Santoro, G.C. King, A constant-time 2D overbodenhausen experiment for inverse correlation of isotopically enriched species, J. Magn. Reson. 97 (1969) 202–207, https://doi.org/10.1016/0022-2364(92)90250-B, 1992.
[34] C. Zwahlen, P. Legault, S.J.F. Vincent, J. Greenblatt, R. Konrat, L.E. Kay, Methods for measurement of intermolecular NOEs by multinuclear NMR spectroscopy: application to a bacteriophage λ N-peptide/*boxB* RNA complex, J. Am. Chem. Soc. 119 (1997) 6711–6721, https://doi.org/10.1021/ja970224q.
[35] R. Fiala, M.L. Munzarová, V. Sklenár, Experiments for correlating quaternary carbons in RNA bases, J. Biomol. NMR 29 (2004) 477–490, https://doi.org/10.1023/B:JNMR.0000034358.12599.d1.
[36] V. Sklenár, H. Miyashiro, G. Zon, H.T. Miles, A. Bax, Assignment of the 31P and 1H resonances in oligonucleotides by two-dimensional NMR spectroscopy, FEBS Lett. 208 (1986) 94–98.
[37] J.P. Marino, H. Schwalbe, C. Anklin, W. Bermel, D.M. Crothers, C. Griesinger, Sequential correlation of anomeric ribose protons and intervening phosphorus in RNA oligonucleotides by a 1H, 13C, 31P triple resonance experiment: HCP-CCH-TOCSY, J. Biomol. NMR 5 (1995) 87–92.
[38] M. Ottiger, F. Delaglio, A. Bax, Measurement of J and dipolar couplings from simplified two-dimensional NMR spectra, J. Magn. Reson. 131 (1998) 373–378, https://doi.org/10.1006/jmre.1998.1361.
[39] A.T. Brünger, P.D. Adams, G.M. Clore, W.L. DeLano, P. Gros, R.W. Grosse-Kunstleve, J.S. Jiang, J. Kuszewski, M. Nilges, N.S. Pannu, R.J. Read, L.M. Rice, T. Simonson, G.L. Warren, Crystallography & NMR system: a new software suite for macromolecular structure determination, Acta Crystallogr. D Biol. Crystallogr. 54 (1998) 905–921.
[40] M. Zweckstetter, G. Hummer, A. Bax, Prediction of charge-induced molecular alignment of biomolecules dissolved in dilute liquid-crystalline phases, Biophys. J. 86 (2004) 3444–3460, https://doi.org/10.1529/biophysj.103.035790.
[41] G.M. Clore, A.M. Gronenborn, N. Tjandra, Direct structure refinement against residual dipolar couplings in the presence of rhombicity of unknown magnitude, J. Magn. Reson. 131 (1998) 159–162, https://doi.org/10.1006/jmre.1997.1345.
[42] W.L. Jorgensen, J. Tirado-Rives, The OPLS [optimized potentials for liquid simulations] potential functions for proteins, energy minimizations for crystals of cyclic peptides and crambin, J. Am. Chem. Soc. 110 (1988) 1657–1666, https://doi.org/10.1021/ja00214a001.
[43] M. Zweckstetter, A. Bax, Prediction of sterically induced alignment in a dilute liquid crystalline phase: aid to protein structure determination by NMR, J. Am. Chem. Soc. 122 (2000) 3791–3792, https://doi.org/10.1021/ja0000908.
[44] L.L.C. Schrödinger, The PyMOL Molecular Graphics System, Version 1.8, 2015.
[45] A.V. Colasanti, X.-J. Lu, W.K. Olson, Analyzing and building nucleic acid structures with 3DNA, JoVE (2013), https://doi.org/10.3791/4401 e4401.
[46] S. Keller, C. Vargas, H. Zhao, G. Piszczek, C.A. Brautigam, P. Schuck, High-precision isothermal titration calorimetry with automated peak-shape analysis, Anal. Chem. 84 (2012) 5066–5073, https://doi.org/10.1021/ac3007522.
[47] M. Molinaro, I. Tinoco, Use of ultra stable UNCG tetraloop hairpins to fold RNA structures: thermodynamic and spectroscopic applications, Nucleic Acids Res. 23 (1995) 3056–3063.
[48] G. Varani, C. Cheong, I. Tinoco, Structure of an unusually stable RNA hairpin, Biochemistry 30 (1991) 3280–3289.
[49] B. Fürtig, C. Richter, W. Bermel, H. Schwalbe, New NMR experiments for RNA nucleobase resonance assignment and chemical shift analysis of an RNA UUCG tetraloop, J. Biomol. NMR 28 (2004) 69–79, https://doi.org/10.1023/B:JNMR.0000012863.63522.1f.
[50] J. SantaLucia, R. Kierzek, D.H. Turner, Context dependence of hydrogen bond free energy revealed by substitutions in an RNA hairpin, Science 256 (1992) 217–219.
[51] M. Katahira, M. Kanagawa, H. Sato, S. Uesugi, S. Fujii, T. Kohno, T. Maeda, Formation of sheared G:A base pairs in an RNA duplex modelled after ribozymes, as revealed by NMR, Nucleic Acids Res. 22 (1994) 2752–2759.
[52] L.B.W. Szewczak, J.S. Gabrielsen, S.J. Degregorio, S.A. Strobel, J.A. Steitz, Molecular basis for RNA kink-turn recognition by the h15.5K small RNP protein, RNA 11 (2005) 1407–1419, https://doi.org/10.1261/rna.2830905.
[53] J. Wang, E.P. Nikonowicz, Solution structure of the K-turn and Specifier Loop domains from the Bacillus subtilis tyrS T-box leader RNA, J. Mol. Biol. 408 (2011) 99–117, https://doi.org/10.1016/j.jmb.2011.02.014.
[54] M. Falb, I. Amata, F. Gabel, B. Simon, T. Carlomagno, Structure of the K-turn U4 RNA: a combined NMR and SANS study, Nucleic Acids Res. 38 (2010) 6274–6285, https://doi.org/10.1093/nar/gkq380.
[55] S. Nottrott, K. Hartmuth, P. Fabrizio, H. Urlaub, I. Vidovic, R. Ficner, R. Lührmann, Functional interaction of a novel 15.5kD [U4/U6.U5] tri-snRNP protein with the 5' stem-loop of U4 snRNA, EMBO J. 18 (1999) 6119–6133, https://doi.org/10.1093/emboj/18.21.6119.
[56] B.S. Tolbert, S.D. Kennedy, S.J. Schroeder, T.R. Krugh, D.H. Turner, NMR structures of (rGCUGAGGCU)2 and (rGCGGAUGCU)2: probing the structural features that shape the thermodynamic stability of GA pairs, Biochemistry 46 (2007) 1511–1522, https://doi.org/10.1021/bi061350m.
[57] X. Shi, L. Huang, D.M.J. Lilley, P.B. Harbury, D. Herschlag, The solution structural ensembles of RNA kink-turn motifs and their protein complexes, Nat. Chem. Biol. 12 (2016) 146–152, https://doi.org/10.1038/nchembio.1997.
[58] T.A. Goody, S.E. Melcher, D.G. Norman, D.M.J. Lilley, The kink-turn motif in RNA is dimorphic, and metal ion-dependent, RNA 10 (2004) 254–264.
[59] K.T. Schroeder, D.M.J. Lilley, Ion-induced folding of a kink turn that departs from the conventional sequence, Nucleic Acids Res. 37 (2009) 7281–7289, https://doi.org/10.1093/nar/gkp791.
[60] S. Matsumura, Y. Ikawa, T. Inoue, Biochemical characterization of the kink-turn RNA motif, Nucleic Acids Res. 31 (2003) 5544–5551.
[61] J. Wang, T. Fessl, K.T. Schroeder, J. Ouellet, Y. Liu, A.D.J. Freeman, D.M.J. Lilley, Single-molecule observation of the induction of k-turn RNA structure on binding L7Ae protein, Biophys. J. 103 (2012) 2541–2548, https://doi.org/10.1016/j.bpj.2012.11.006.
[62] H. Workman, J.J. Skalicky, P.F. Flynn, Assignment of 1H, 13C, and 15N resonances of the RNA binding protein Snu13p from Saccharomyces cerevisiae, Biomol. NMR Assignments 2 (2008) 1–3, https://doi.org/10.1007/s12104-007-9069-1.
[63] C. Charron, X. Manival, B. Charpentier, C. Branlant, A. Aubry, Purification, crystallization and preliminary X-ray diffraction data of L7Ae sRNP core protein from Pyrococcus abyssii, Acta Crystallogr. D Biol. Crystallogr. 60 (2004) 122–124.
[64] S. vdya Oruganti, Y. Zhang, H. Li, Structural comparison of yeast snoRNP and spliceosomal protein Snu13p with its homologs, Biochem. Biophys. Res. Commun. 333 (2005) 550–554, https://doi.org/10.1016/j.bbrc.2005.05.141.
[65] C. Charron, X. Manival, A. Cléry, V. Senty-Ségault, B. Charpentier, N. Marmier-Gourrier, C. Branlant, A. Aubry, The archaeal sRNA binding protein L7Ae has a 3D structure very similar to that of its eukaryal counterpart while having a broader RNA-binding specificity, J. Mol. Biol. 342 (2004) 757–773, https://doi.org/10.1016/j.jmb.2004.07.046.
[66] H.C. Dobbyn, P.A. McEwan, A. Krause, L. Novak-Frazer, J. Bella, R.T. O'Keefe, Analysis of pre-mRNA and pre-rRNA processing factor Snu13p structure and mutants, Biochem. Biophys. Res. Commun. 360 (2007) 857–862, https://doi.org/10.1016/j.bbrc.2007.06.163.
[67] J. Lin, S. Lai, R. Jia, A. Xu, L. Zhang, J. Lu, K. Ye, Structural basis for site-specific ribose methylation by box C/D RNA protein complexes, Nature 469 (2011) 559–563, https://doi.org/10.1038/nature09688.
[68] H.C. Dobbyn, R.T. O'Keefe, Analysis of Snu13p mutations reveals differential interactions with the U4 snRNA and U3 snoRNA, RNA 10 (2004) 308–320.
[69] A. Mougin, A. Gottschalk, P. Fabrizio, R. Lührmann, C. Branlant, Direct probing of RNA structure and RNA-protein interactions in purified HeLa cell's and yeast spliceosomal U4/U6.U5 tri-snRNP particles, J. Mol. Biol. 317 (2002) 631–649, https://doi.org/10.1006/jmbi.2002.5451.
[70] S. Granneman, G.J.M. Pruijn, W. Horstman, W.J. van Venrooij, R. Luhrmann,

N.J. Watkins, The hU3-55K protein requires 15.5K binding to the box B/C motif as well as flanking RNA elements for its association with the U3 small nucleolar RNA in Vitro, J. Biol. Chem. 277 (2002) 48490–48500, https://doi.org/10.1074/jbc.M206631200.

[71] A. Cléry, V. Senty-Ségault, F. Leclerc, H.A. Raué, C. Branlant, Analysis of sequence and structural features that identify the B/C motif of U3 small nucleolar RNA as the recognition site for the Snu13p-Rrp9p protein pair, Mol. Cell Biol. 27 (2007) 1191–1206, https://doi.org/10.1128/MCB.01287-06.

[72] B. Rothé, X. Manival, N. Rolland, C. Charron, V. Senty-Ségault, C. Branlant, B. Charpentier, Implication of the box C/D snoRNP assembly factor Rsa1p in U3 snoRNP assembly, Nucleic Acids Res. 45 (2017) 7455–7473, https://doi.org/10.1093/nar/gkx424.

[73] S. Boulon, N. Marmier-Gourrier, B. Pradet-Balade, L. Wurth, C. Verheggen, B.E. Jády, B. Rothé, C. Pescia, M.-C. Robert, T. Kiss, B. Bardoni, A. Krol, C. Branlant, C. Allmang, E. Bertrand, B. Charpentier, The Hsp90 chaperone controls the biogenesis of L7Ae RNPs through conserved machinery, J. Cell Biol. 180 (2008) 579–595, https://doi.org/10.1083/jcb.200708110.

[74] B. Rothé, J.-M. Saliou, M. Quinternet, R. Back, D. Tiotiu, C. Jacquemin, C. Loegler, F. Schlotter, V. Peña, K. Eckert, S. Moréra, A.V. Dorsselaer, C. Branlant, S. Massenet, S. Sanglier-Cianférani, X. Manival, B. Charpentier, Protein Hit1, a novel box C/D snoRNP assembly factor, controls cellular concentration of the scaffolding protein Rsa1 by direct interaction, Nucleic Acids Res. 42 (2014) 10731–10747, https://doi.org/10.1093/nar/gku612.

[75] G. Chanfreau, G. Rotondo, P. Legrain, A. Jacquier, Processing of a dicistronic small nucleolar RNA precursor by the RNA endonuclease Rnt1, EMBO J. 17 (1998) 3726–3737, https://doi.org/10.1093/emboj/17.13.3726.

[76] L. Huang, S. Ashraf, D.M.J. Lilley, The role of RNA structure in translational regulation by L7Ae protein in archaea, RNA (2018), https://doi.org/10.1261/rna.068510.118.

[77] D. Jäger, K.U. Förstner, C.M. Sharma, T.J. Santangelo, J.N. Reeve, Primary transcriptome map of the hyperthermophilic archaeon Thermococcus kodakarensis, BMC Genom. 15 (2014) 684, https://doi.org/10.1186/1471-2164-15-684.

[78] L. Huang, S. Ashraf, J. Wang, D.M. Lilley, Control of box C/D snoRNP assembly by N6-methylation of adenine, EMBO Rep. 18 (2017) 1631–1645, https://doi.org/10.15252/embr.201743967.

[79] D.A. Samarsky, M.J. Fournier, R.H. Singer, E. Bertrand, The snoRNA box C/D motif directs nucleolar targeting and also couples snoRNA synthesis and localization, EMBO J. 17 (1998) 3747–3757, https://doi.org/10.1093/emboj/17.13.3747.

[80] V. Cojocaru, S. Nottrott, R. Klement, T.M. Jovin, The snRNP 15.5K protein folds its cognate K-turn RNA: a combined theoretical and biochemical study, RNA 11 (2005) 197–209, https://doi.org/10.1261/rna.7149605.